Supporting Information

High stability $SrTi_{1-x}Fe_xO_{3-\delta}$ electrodes for oxygen reduction and oxygen evolution reactions

Shan-Lin Zhang,[a,b] Dalton Cox,[a] Hao Yang,[b] Beom-Kyeong Park,[a] Cheng-Xin Li,[b] Chang-Jiu Li,[b] Scott A. Barnett [a,*]

[a.] Department of Materials Science and Engineering, Northwestern University, Evanston, Illinois 60208, USA. E-mail: s-barnett@northwestern.edu

[b.] State Key laboratory for Mechanical Behavior of Materials, School of Materials Science and Engineering, Xi'an Jiaotong University, Xi'an, Shaanxi, 710049, People's Republic of China. E-mail: licj@xjtu.edu.cn

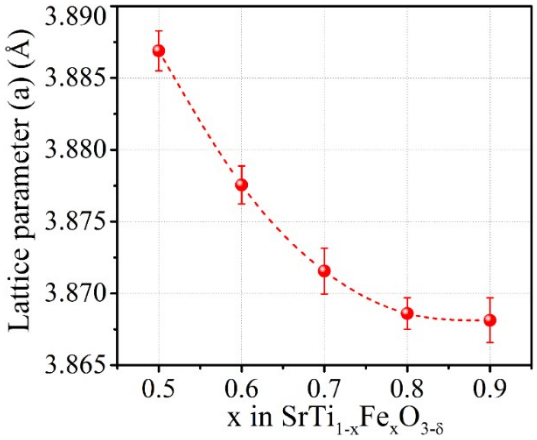

Fig. S1 Variation in lattice parameter with Ti/Fe ratio

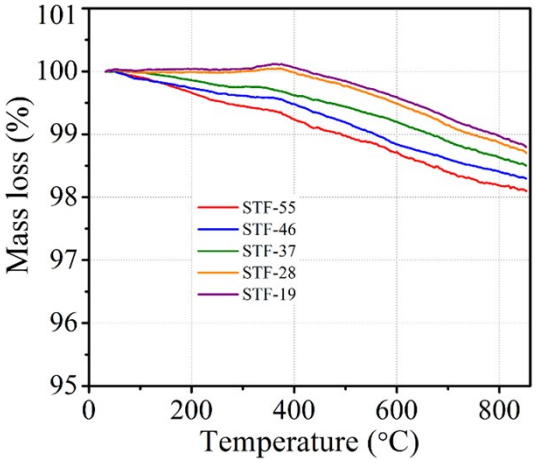

Fig. S2 Thermogravimetric analysis of STF powders under air atmosphere

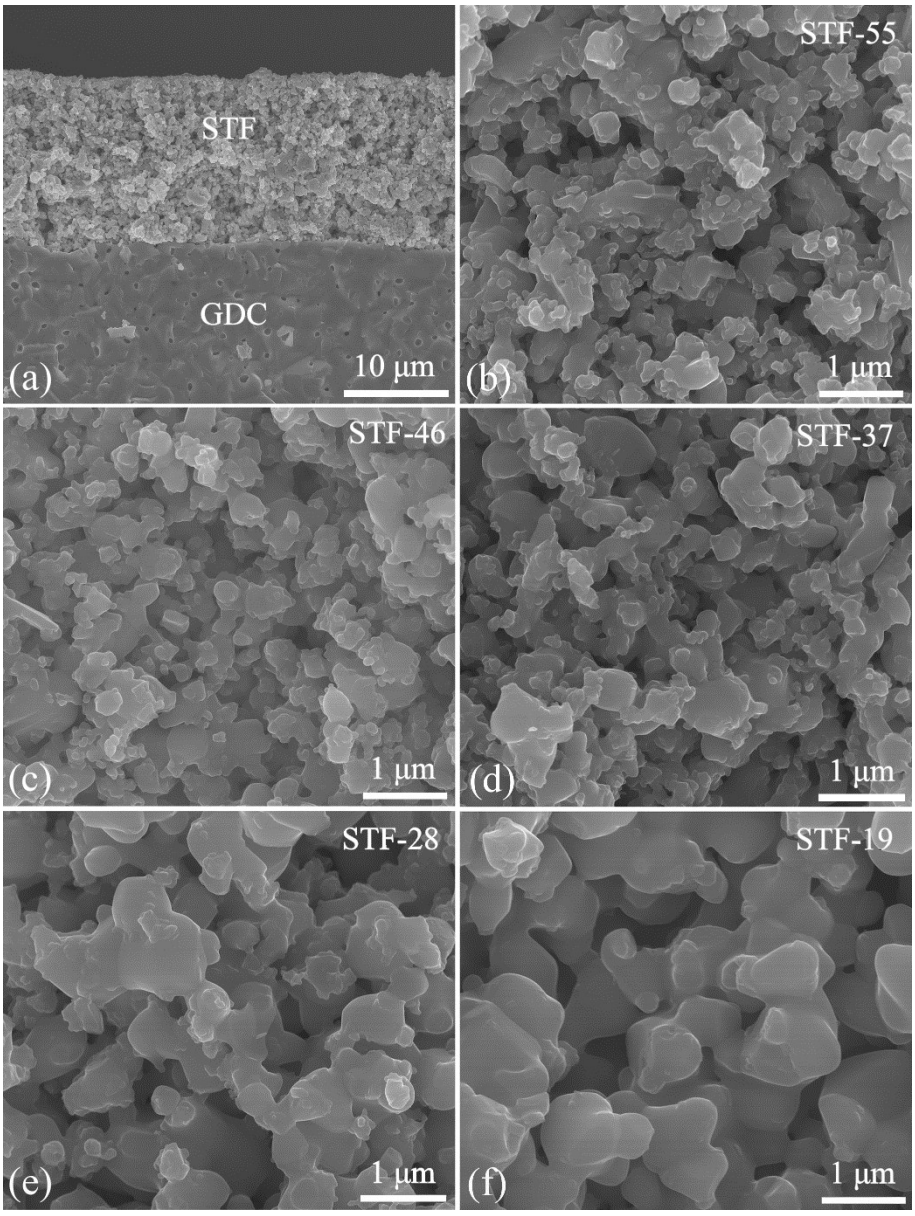

Fig. S3 Microstructure of screen printed STF electrodes. (a) Low magnification image for STF-37; High magnification image for STF-55 (b), STF-46 (c), STF-37 (d), STF-28 (e), and STF-19 (f).

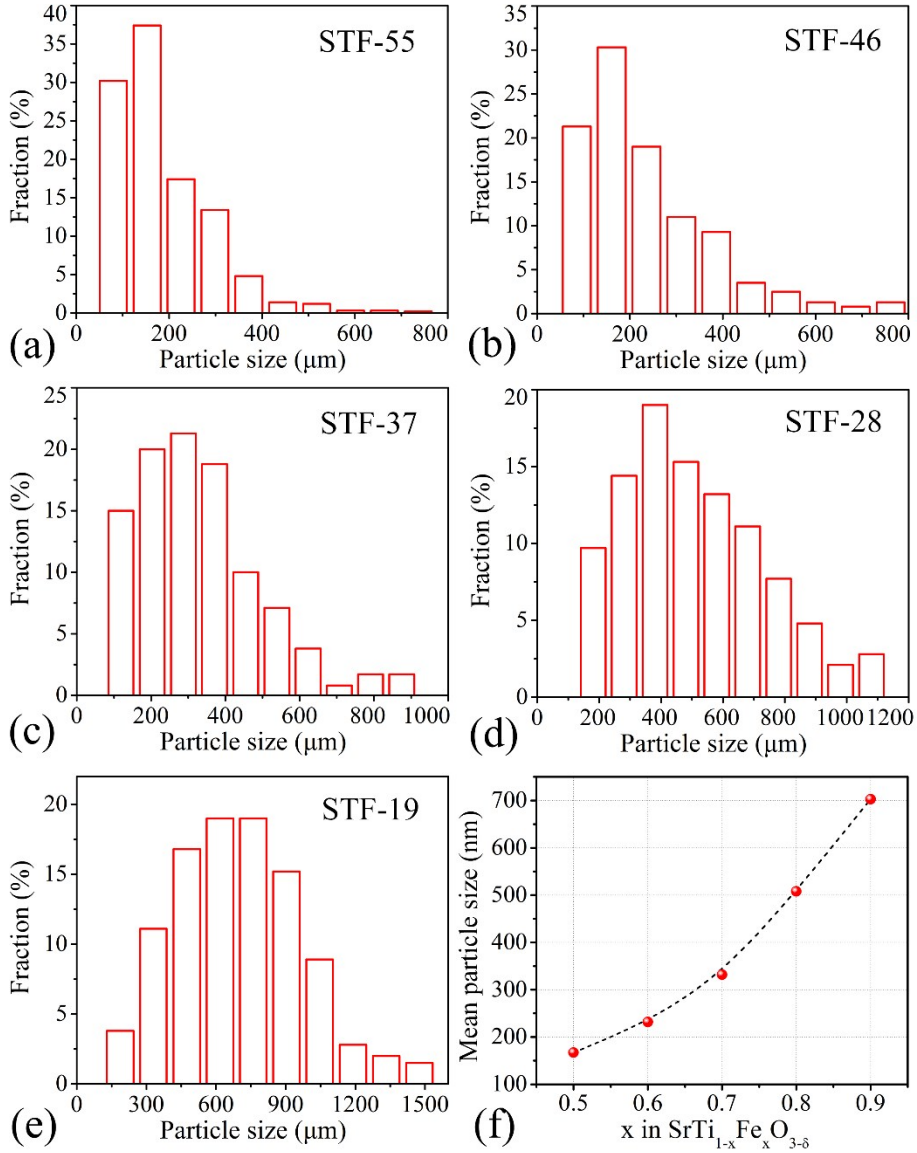

Fig. S4 Particle size distribution obtained from the microstructure (a) STF-55, (b) STF-46, (c) STF-37, (d) STF-28, and (e) STF-19; (f) Mean particle size of different STF.

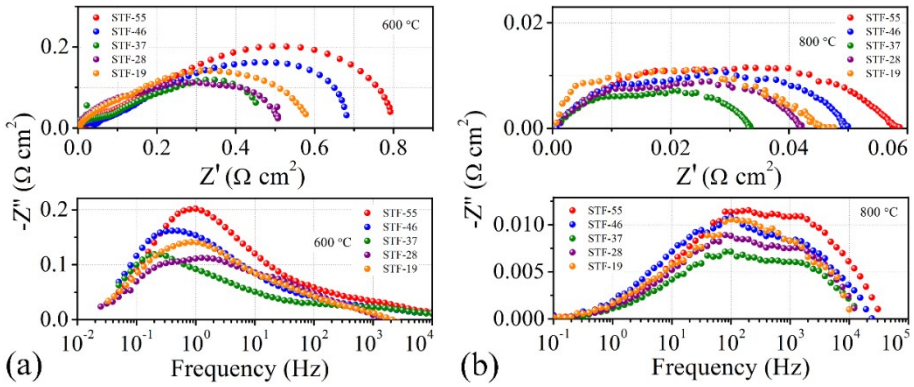

Fig. S5 Typical Nyquist and Bode plots of EIS data for the symmetrical cells measured at 600 °C (a) and 800 °C (b).

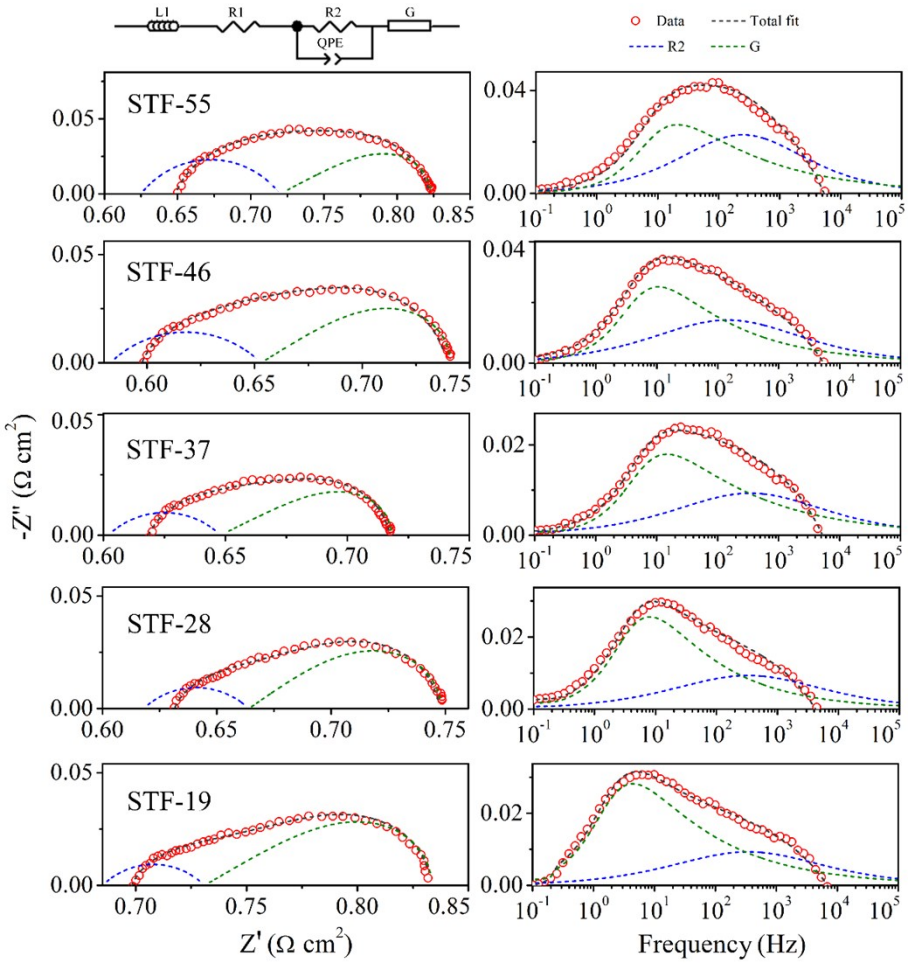

Fig. S6 Typical L-R-G EIS fittings for the symmetric cells at 700 °C. Left: Nyquist plots; Right: Bode plots. Dot lines are the fitting results. Note that the inductance of test setup wires is not shown as a separate response in these plots, and is responsible for the apparent difference between the overall fit and the individual responses.

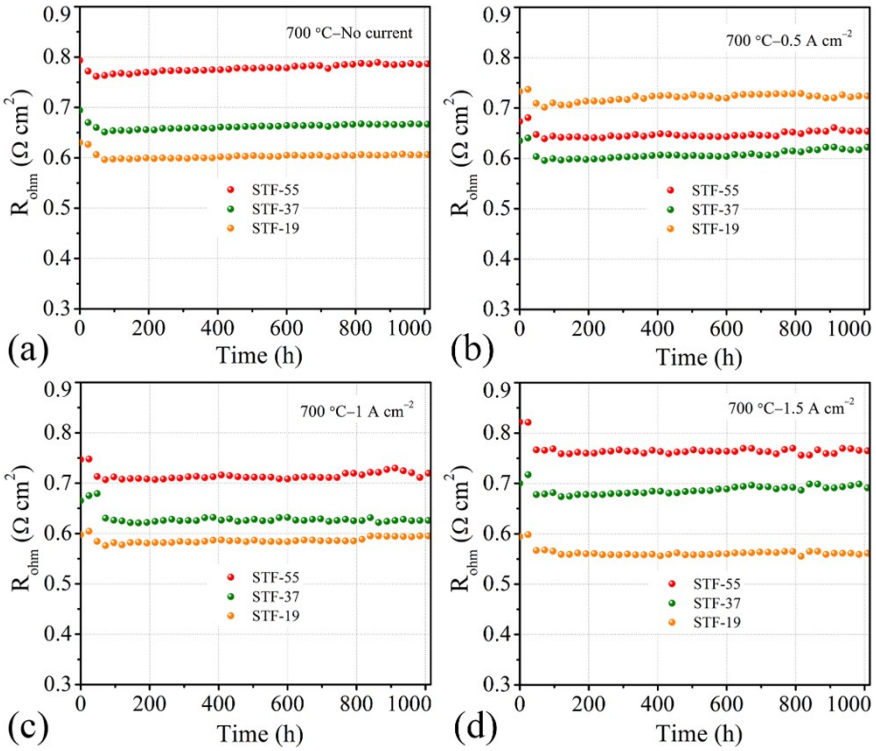

Fig. S7 Ohmic resistance *versus* time for the symmetric cells with STF electrodes during life testing at 700 °C; (a) without current; (b) 0.5 A cm^{-2} current; (c) 1 A cm^{-2} current; (d) 1.5 A cm^{-2} current. A small difference between the initial values attributed to the small difference of the thickness of GDC electrolytes.

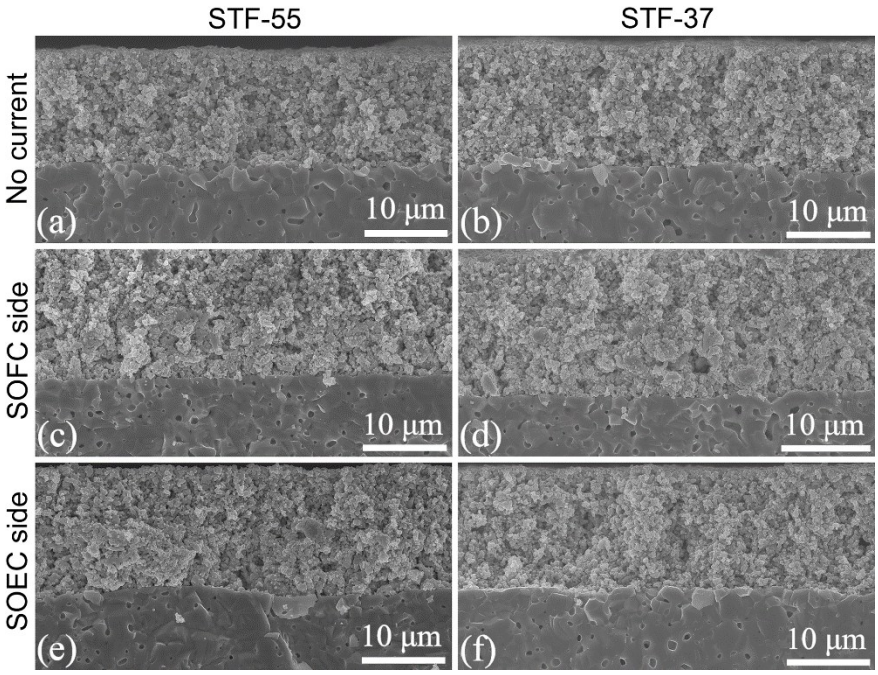

Fig. S8 Fracture cross sectional images of the cells with STF-55 (left) and STF-37 (right) electrodes after 1000 h test; (a) and (b) without current, (c) and (d) SOFC side after running 1.5 A cm^{-2} current, (e) and (f) SOEC side after running 1.5 A cm^{-2} current.

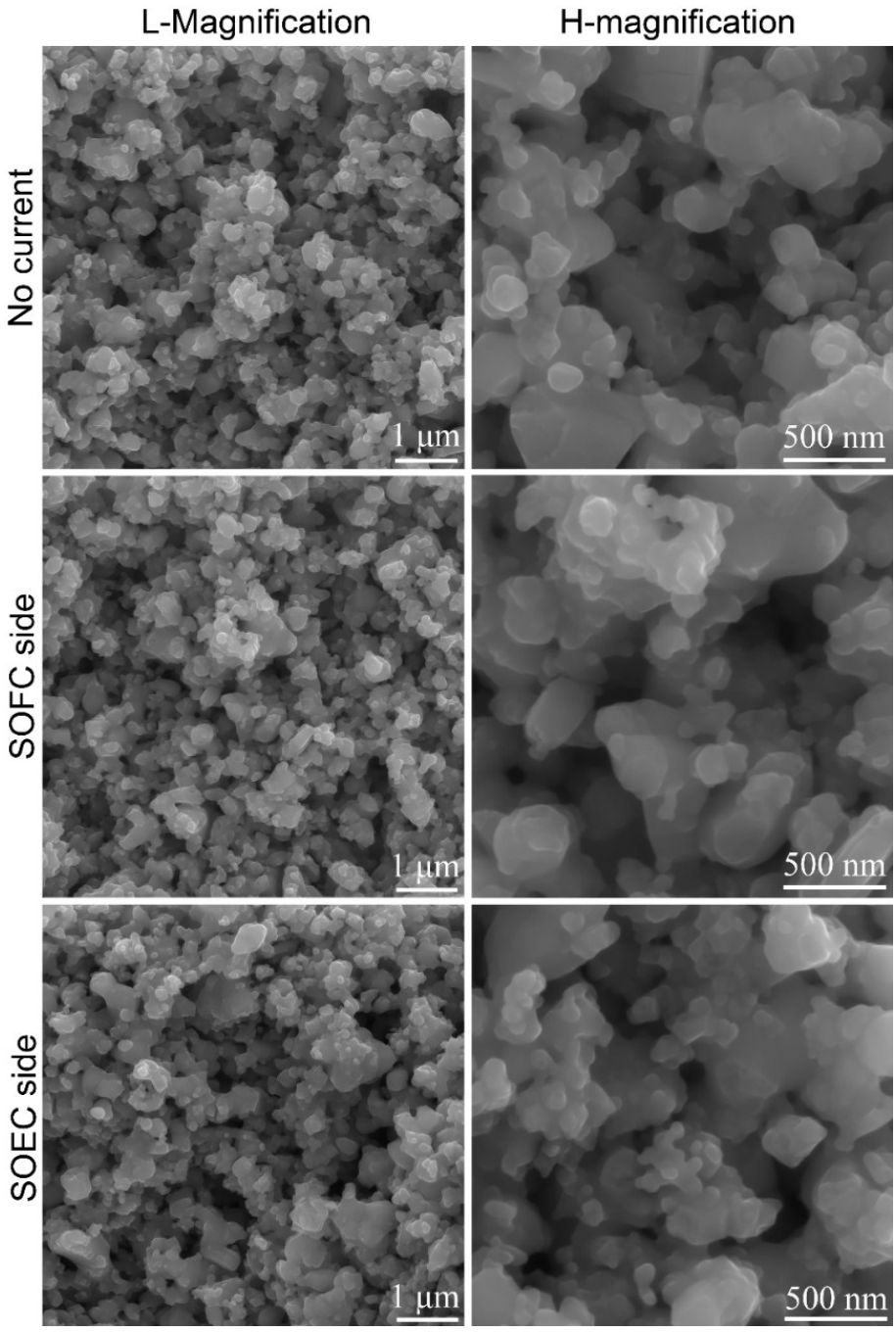

Fig. S9 Fractured surface morphologies for symmetric cells with STF-55 electrodes after the ageing (700 °C, without current and 1.5 A cm^{-2} current). Left: low-magnification images; right: high-magnification images.

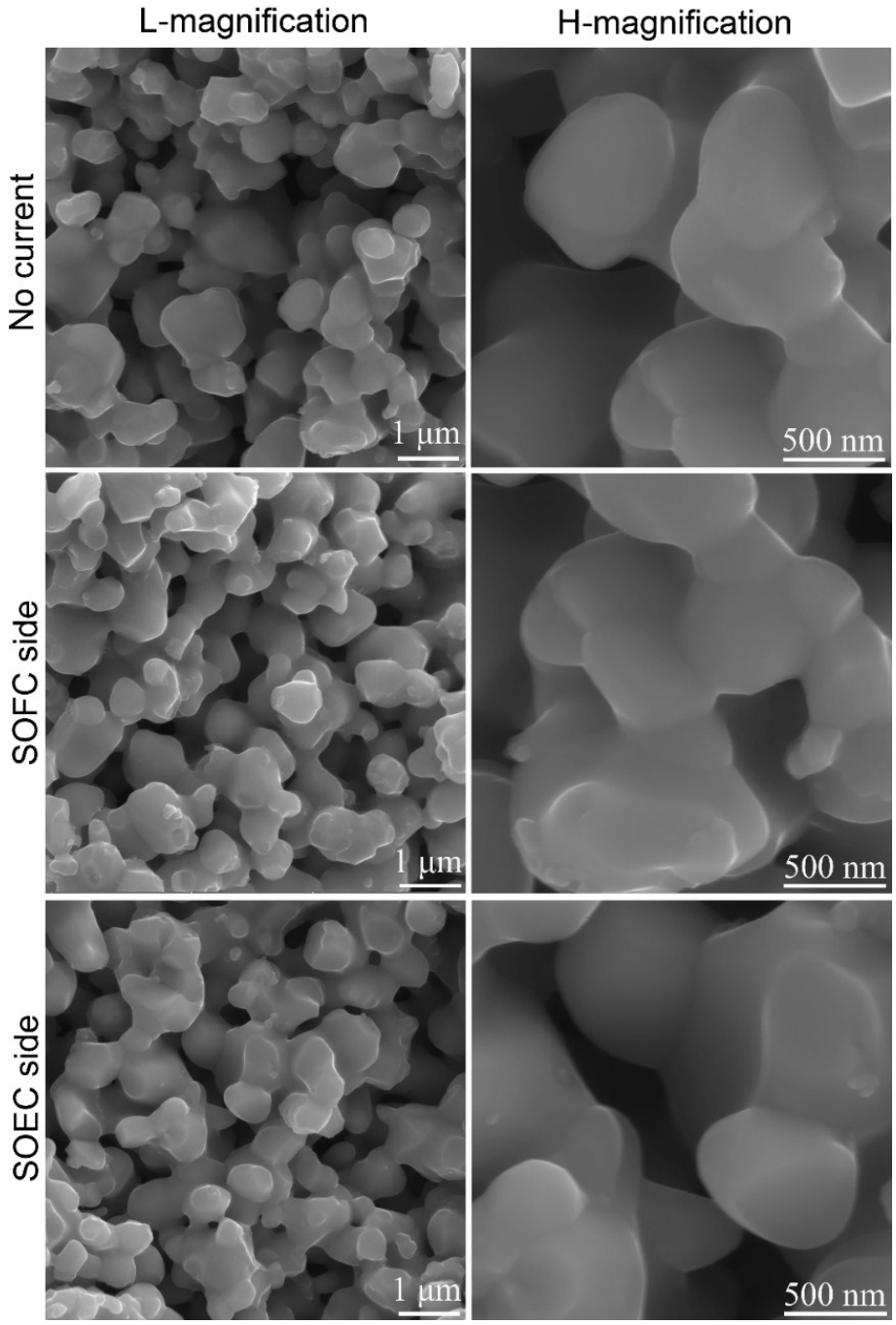

Fig. S10 Fractured surface morphologies for symmetric cells with STF-19 electrodes after the ageing (700 °C, without current and 1.5 A cm^{-2} current). Left: low-magnification images; right: high-magnification images.

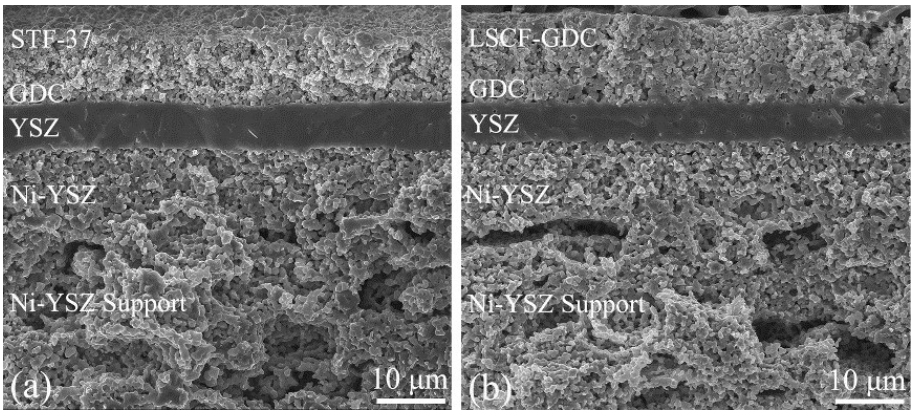

Fig. S11 Cross section SEM image of the full cells after performance testing; (a) with STF-37 electrode; (b) with LSCF-GDC electrode.

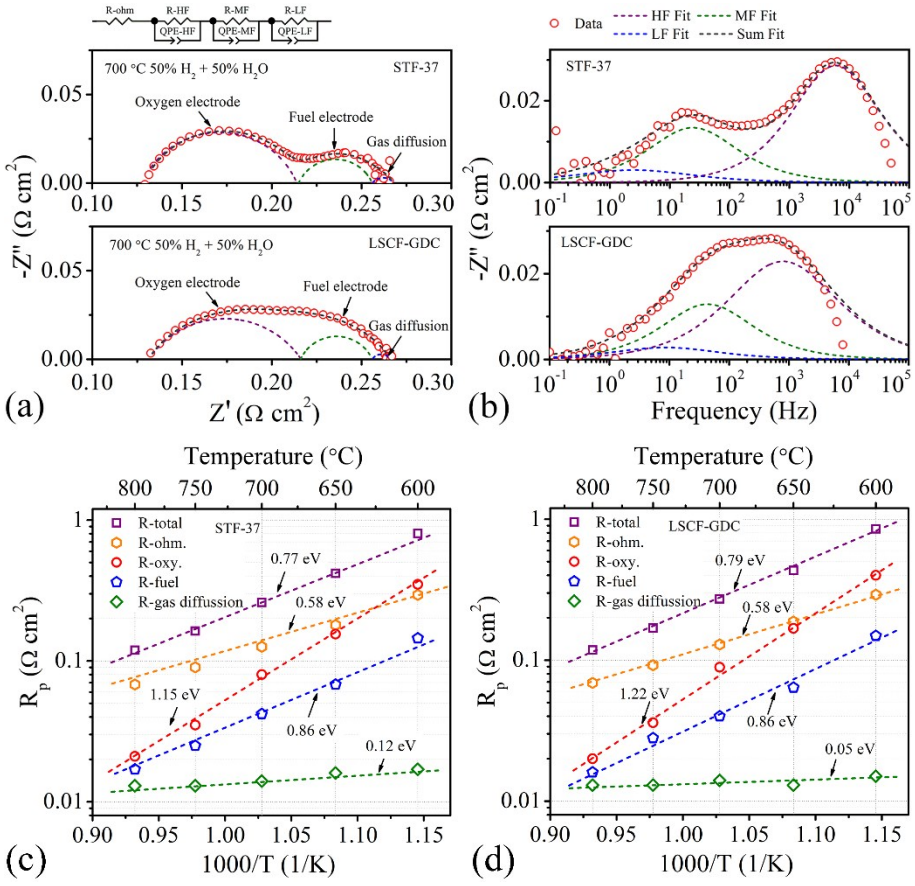

Fig. S12 Equivalent circuit fits for EIS data (700 °C, 50% H_2O + 50% H_2) from full cells; (a) Nyquist and (b) Bode plots; Arrhenius plots of the polarization resistances from the fitting results for the full cells (c) with STF-37 electrode and (d) with LSCF/GDC electrode.

Discussion of the full cell EIS data

In this study, the cell exhibited three clear impedance responses at all the temperatures. The EIS data was fit to an equivalent circuit consisting of three RQ elements, matching to the three different responses seen by visual inspection, an Ohmic resistance (R_{ohm}), and an inductor. Fig. S12 (a) and (b) shows typical fits, for data taken at 700 °C. The resistance values obtained from each circuit element are shown in the Arrhenius plots in Fig. S12 (c) and (d). The Ohmic resistance values are consistent with the magnitude expected for the YSZ electrolyte, although the activation energy is lower than expected. The response at ~1–10 Hz did not vary significantly with temperature (Fig. S10 (c) and (d)), and is therefore associated with gas diffusion in the thick support. The response peaking at ~300 Hz is a combination of the Ni–YSZ fuel electrode response. For STF-37 cell, the response peaking at ~10^4 Hz is the oxygen electrode response. While for LSCF-GDC cell, the oxygen electrode response is mainly at ~10^3 Hz. However, for both two cells, the high frequency response seen in the cathode full cell EIS data is larger than that in symmetric cells. This may be due to a difference in the processing between the symmetric in full cells, or there may be an additional interfacial resistance in the full cells that is not present in the symmetric cells. Even there is a litter difference on the oxygen electrode response peaking, the resistance values from each part are very close for two type cells.

Table S1 Oxygen non-stoichiometry (δ) values obtained from Fig. 1 (d)

Temperature	STF-55	STF-46	STF-37	STF-28	STF-19
600	0.215	0.236	0.243	0.259	0.288
650	0.233	0.250	0.261	0.288	0.306
700	0.252	0.263	0.271	0.310	0.326
750	0.266	0.276	0.295	0.328	0.345
800	0.277	0.287	0.310	0.342	0.361

Table S2 Time constant t_G (s) values obtained from fitting the EIS data and used in the ALS model calculations

Temperature	STF-55	STF-46	STF-37	STF-28	STF-19
600	0.2180	0.251	0.214	0.458	0.923
650	0.0437	0.0375	0.0428	0.101	0.231
700	0.0094	0.0125	0.0143	0.035	0.0846
750	0.0028	0.0063	0.007	0.0125	0.0231
800	0.0013	0.0025	0.0021	0.0067	0.0131

Table S3 Gerischer resistance RG (Ω cm^2) values obtained from fitting the EIS data and used in the ALS model calculations

Temperature	STF-55	STF-46	STF-37	STF-28	STF-19
600	0.721	0.583	0.407	0.45	0.498
650	0.261	0.201	0.145	0.16	0.199
700	0.103	0.088	0.071	0.084	0.102
750	0.052	0.055	0.041	0.041	0.047
800	0.031	0.032	0.021	0.029	0.032

Table S4 Solid-phase tortuosity obtained from 2D microstructure analysis used in the ALS model calculations

Electrodes	STF-55	STF-46	STF-37	STF-28	STF-19
τ	1.1943	1.2348	1.1757	1.2113	1.1233

Stereological Analysis

2D stereological analyses of the oxygen electrode microstructures were performed to obtain specific surface area and porosity. Polished epoxy-infiltrated samples were milled and imaged at 8000x magnification using an FEI Helios FIB-SEM. Images of the electrode were taken in a manner to avoid biasing the results: there was no overlap in images in the x-y plane and milling depth in the z direction was greater than the largest particle size to ensure independence of the sampled areas.

Using in-house MATLAB code, the SEM images (Fig. 2(b)-(f)) were binaried into solid and pore phases and the total length of interface of the two phases in each 2D image was calculated. Porosity and specific surface area were estimated using the equations:

$$\varepsilon = \varepsilon_A \tag{S1}$$

$$a = \frac{4}{\pi} L_A \tag{S2}$$

Where ε_A is the 2D porosity of the image and L_A is the interface length divided by the area of the image[1]. Values obtained for each image were averaged within the composition dataset. To verify the method, the stereological calculations were performed on previously obtained full 3D reconstruction datasets. It was found that 10 independent images (no particle overlap between images) of the 300 image datasets was sufficient to ensure that 3D porosity and surface area values fell within the error of stereological measurement.

Reference

[1] C.V. Howard, M.G. Reed, Unbiased Stereology: Three-Dimensional Measurement in Microscopy, 1999.